

Morphology and Evolution of the LMC Planetary Nebulae¹

Richard A. Shaw, Letizia Stanghellini², Max Mutchler
Space Telescope Science Institute, Baltimore, MD 21218
 shaw@stsci.edu, lstanghe@stsci.edu, mutchler@stsci.edu

Bruce Balick
University of Washington, Seattle, WA 98195
 balick@astro.washington.edu
 and

J. Chris Blades
Space Telescope Science Institute, Baltimore, MD 21218
 blades@stsci.edu

ABSTRACT

The LMC is ideal for studying the co-evolution of planetary nebulae (PNe) and their central stars, in that the debilitating uncertainties of the Galactic PN distance scale and selection biases from attenuation by interstellar dust do not apply. We present images and analyze slit-less spectra which were obtained in a survey of Large Magellanic Cloud PNe. These data on 29 targets were obtained with *HST* using the Space Telescope Imaging Spectrograph. The data permit us to determine the nebular dimensions and morphology in the monochromatic light of several emission lines, including those that have traditionally been used for morphological studies in the Galaxy: $H\alpha$, $[N\ II] 6583\ \text{\AA}$ and $[O\ III] 5007\ \text{\AA}$, plus others of varying ionization, including $[O\ I]$, He I, and $[S\ II]$. Together with the 31 resolved LMC PNe for which monochromatic images exist in the *HST* archive, these data show that the incidence of non-symmetric nebulae, including bipolar nebulae (which is an indicator of Population I ancestry in the Galaxy), is significantly higher than that reported for the Galaxy. The onset of asymmetric features appears even in very young nebulae (with dynamical ages of ~ 1400 yr), suggesting that at least the gross features of the nebular morphology may be more closely tied to PN formation, and that subsequent shaping of the expanding envelope by the radiation field and wind from the central star may play the lesser role of amplifying these gross features. There is some evidence of evolution between two morphological types, in the sense that bipolar core (BC) nebulae may evolve to pure bipolars late in the PN lifetime.

Subject headings: Planetary Nebulae; Morphology, Evolution – Magellanic Clouds

²Affiliated with the Astrophysics Division, Space Science Department of ESA; on leave from Osservatorio Astronomico di Bologna

¹Based on observations with the NASA/ESA Hubble Space Telescope, obtained at the Space Telescope Science Institute, which is operated by the Association of Universi-

1. Introduction

The nature of the physical connection between planetary nebulae (PNe) and their central stars

ties for Research in Astronomy, Inc., under NASA contract NAS 5-26555.

has been studied for the better part of the last century, and a good deal of physical insight into the late stages of stellar evolution has emerged as a consequence. As images have improved, it has become surprisingly clear that mass loss is far from isotropic. These and other observations have challenged our understanding of the formation of PNe, and of the role of their central stars (CSs) in the subsequent evolution of the shells. This latter topic has received a great deal of attention in the past three decades, driven by the availability of new techniques in observing and in theoretical modelling. That the shapes of the ejected PN shells should somehow relate to the formation mechanism is perhaps easy to intuit, but the connection between nebular morphology and the Population type of the progenitor stars (Greig 1972) is not so easy to understand. Subsequent work by many investigators (e.g., Peimbert 1978; Peimbert & Torres-Peimbert 1983; Kaler 1983, to name but a few) began to connect nebular abundances to the results of stellar evolution processes in the central stars immediately prior to PN formation. It is primarily from these connections that the relationship between asymmetric PNe and higher CS (and progenitor star) mass can be inferred.

But what is it, exactly, that PN morphologies tell us about their formation history? How can we relate morphology to the physical properties of the nebulae, their environments, and especially their CSs? In principle, morphology should reflect one or more factors, which we might characterize as either “local” — relating to properties of the CS and the immediate vicinity at the time of formation — or “non-local” — relating to conditions that exist or develop after the PN is formed. Local properties would include the dynamics of the gas at the moment of ejection, departures from spherical symmetry of the gravitational or magnetic field immediately surrounding the CS, and by the amount of dust within the expelled gas. Non-local properties include the circumstellar environment, including mass ejected from the CS prior to the PN ejection and the density of the local ISM, and the radiation field and wind from the CS, both of which change rapidly as the star evolves to a white dwarf. Balick (1987) presented compelling evidence for a restricted sample of Galactic PNe that nebular morphologies can be greatly influenced by the energy (from wind and radiation) deposited in

the nebula by the CS. What was lacking most was a sense of the relative importance of local vs. non-local factors on nebular morphology, and whether the influence of these factors varied with morphological type. While comprehensive catalogs of PNe have been available for some time (e.g. Acker, et al. 1982), no systematic morphological classification scheme on a large PN sample was published before the 1990s.

In the early part of the last decade Schwarz, Corradi, & Melnick (1992) published a catalog of nearly 300 southern Galactic PNe, and a few years later a similar effort was completed by Manchado, et al. (1996) for 243 northern PNe. More recently, Górný, et al. (1999) published a catalog of an additional 100 southern PNe. Combined with earlier, more limited image catalogs, these large databases are proving essential for defining and refining the morphological classes, and for deriving their statistical properties. A number of papers based on these catalogs lead to a new view of PN formation, and how it is related to the evolution of the progenitor stars (Stanghellini, Corradi, & Schwarz 1993; Corradi & Schwarz 1995). The interpretation that emerged was that PN morphology is an essential physical property, linked to details of the progenitor formation (i.e., the parent stellar population), the main sequence mass and evolution of the progenitor, and the dynamical evolution of the nebula once it was formed. In particular, it confirmed that progenitors of the most asymmetric PNe belong to a younger stellar population than those that form elliptical or round PNe, that they are on average more massive and produce more massive central stars, and that the nebulae are rich in nitrogen but are relatively carbon-poor compared with most PNe.

Many of the important physical properties that one can derive from observations of a PN and its central star, including the nebular dimensions, mass, dynamical age, and the stellar luminosity and mass, depend upon the correct determination of their distances. But the distances to Galactic PNe have been problematic for decades, as relatively few individual PN distances are accurately determined. Typically, statistical methods of distance determination have been used to derive these important properties, in spite of the difficulty of distinguishing nebulae that are optically thick from those that are optically thin to H

ionizing radiation, where different statistical techniques are employed. But even if these statistical distances were accurate for a given PN sample, it is often hard to draw conclusions when the PN sample so derived is small—e.g., when dealing with rare morphologies such as point-symmetric PNe. Studies of Galactic PNe are also vulnerable to selection biases, such as extinction through the Galactic plane that can make certain PN populations more difficult to observe. For instance, bipolar PNe (and asymmetric PNe in general) are more concentrated in the Galactic disk, with a scale height of roughly half that of symmetric (round or elliptical) PNe (Manchado, et al. 2000). Thus asymmetric PNe are somewhat more affected by interstellar extinction, and are more likely to fall below detection thresholds. In principle, the sample of asymmetric PNe could be significantly under-represented, rendering statistical comparisons between symmetric and asymmetric PNe less valid.

The idea of investigating the morphologies of PNe in the Magellanic Clouds arises from these difficulties, but it requires *HST* imaging to determine their classifications with certainty. *HST* observations of LMC PNe began with an early program by Blades, et al. (1992), and was followed up by Dopita, et al. (1996) and Vassiliadis, et al. (1998). Unfortunately, all of these observations were acquired with the spherically aberrated *HST* before the first servicing mission in 1993, which limits their utility. Stanghellini, et al. (1999) summarized these observations and expanded the analysis of these data to study the LMC PN morphologies. Another, more recent set of LMC PN images were acquired by Dopita (*HST* Program 6407), but to date they have not been published.

Our Cycle 8 program (ID: 8271), a snapshot survey using STIS slit-less spectroscopy, both dramatically enlarges the existing pool of LMC PN images obtained with *HST*, and provides the most complete information on extra-galactic PN morphology achieved to date. This is because our observing technique yields the shape of the PNe in several prominent recombination and forbidden lines, in addition to the line fluxes, thus giving morphological and spectral information at once. With the fruits of our survey we can use morphology as an independent parameter to search for relationships between the physics of the nebulae and

their progenitor stars, and we can do this better than in prior surveys. The survey is 58% complete, but the observing policy for SNAPSHOT observations with *HST* means that few of the remaining targets are likely to be observed. If more PNe are observed in the future, we will include and analyze them in subsequent papers.

While the major motivations for this LMC survey was the detection of PN morphology in a sample that was free of distance- and extinction-biases, this was not the only motivation. The different metallicity of the LMC and the Galaxy allows a comparative study of PN formation and evolution in environments where the initial (progenitor) chemistry differ. An planned extension of our program to the SMC will permit an exploration of these effects with an even larger metallicity baseline.

In this paper we describe our program, from planning to results, and we focus on the morphology of the nebulae and their peculiarities. In §2 we describe our dataset, including the target selection criteria, the observing techniques, and the calibration process used to obtain the images of the figures. In §3 we describe our morphological classification, the nebular dimensions, and comment on individual characteristics of the nebulae. Section 4 discusses the morphology in relation to the evolution of the nebulae, explores the variation of nebular expansion velocity with size and morphology, and concludes with comments on selection effects and other caveats. Section 5 presents the conclusions and looks forward to future projects.

2. The LMC PN Dataset

2.1. Target Selection

The main tactical thrust of our program is to determine the morphology of a large number of PNe in the monochromatic light of a number of important emission lines, and to determine the chemical abundances from ground-based spectroscopy. Since *HST* images are the most expensive and critical commodity, we needed to make maximum use of existing images in the Hubble Data Archive, in spite of the poor quality of some of the images (which were affected by spherical aberration), and the lack of images in the continuum and in low-ionization lines (Stanghellini, et al. 1999). We elected not to include these targets in our survey,

but they may be worth re-observing in the future.

In view of the aim of our scientific project, to correlate morphology with the physical and chemical characteristics of the nebulae, their central stars, and their immediate environment, we required moderate resolution spectroscopy for all PNe in our survey. For this reason, and to help maximize the chance that our selected targets were genuine PNe, we selected where possible PNe with published spectra, either from ground-based or (ideally) from *HST* observations. We also ensured that our sample was widely spread over the face of the LMC in order to explore any relationships that might exist between properties of the nebulae and location within that galaxy. These constraints still left us with a large number of candidate targets, so that we were free to exclude PNe in exceptionally crowded fields of bright sources: such contamination is particularly problematic for slit-less spectroscopy. But in the end, the major constraints in our target selection were the restrictions that apply to “snapshot” program with *HST*, the most severe of which is that they are limited to one orbit per visit; in general, the available exposure time is constrained to $\lesssim 40$ min, minus instrument overheads. Within these limits, we tried to select a sample of 50 PNe, out of the few hundred PNe known in the LMC (Leisy, et al. 1997), which spanned as large a range as possible in the [O III] and H α line fluxes in order to cover as large a range as possible of nebular age and other properties.

2.2. Observations

The data presented here were obtained with *HST* using the Space Telescope Imaging Spectrograph (STIS). The design for this instrument was described by Woodgate, et al. (1998), and the initial on-orbit performance was summarized by Kimble, et al. (1998). All of our observations were made with the CCD detector, using a gain of 1 e^- /ADU. Most of our exposures were split into two equal components to facilitate cosmic ray removal. We obtained slit-less spectra with the G430M and G750M gratings which yielded monochromatic images of the sample nebulae in several important emission lines. We also obtained direct, broad-band images with the clear (50CCD) aperture in order to measure central star magnitudes as faint as $V \approx 24$ with a short exposure,

and to distinguish between the spatial and the velocity structure in extended and/or rapidly expanding nebulae. The observing log is presented in Table 1.

The STIS CCD plate scale of $0''.051 \text{ pixel}^{-1}$ yields a physical scale of $\approx 0.025 \text{ pc pixel}^{-1}$, which is comparable to ground-based images of Galactic PNe. Only one of the nebulae in our sample had been previously resolved from the ground, and few emission line fluxes beyond H β 4861 Å and [O III] 4959, 5007 Å had been published. We therefore planned our exposures to achieve a signal-to-noise ratio of ~ 30 per pixel for a typical nebula of $0''.5$ in diameter and a roughly uniform surface brightness distribution, but we bracketed our exposure times where possible to avoid saturation (for angularly small nebulae) while still providing sufficient signal (for large nebulae) to make a good morphological classification. Finally, the limitations of *HST* “snapshot” programs (e.g., a maximum of one orbital period per target) meant that the G430M exposure for the faintest target, LMC-J 41, had to be omitted in favor of a strong detection in G750M.

The G750M spectra cover the wavelength range from 6295–6865 Å, which includes emission from H α 6563 Å and [N II] 6548, 6583 Å: these are the primary lines used for morphological classification. For those nebulae with relatively high surface brightness, the exposures also contain monochromatic images of [S II] 6717, 6731 Å, He I 6678 Å, and (for low-ionization nebulae) [O I] 6300, 6363 Å. Together, these lines reveal the low- to moderate-ionization morphological features, which are the most important for tracing the earliest phase of the morphological evolution of the nebulae. The mean dispersion for G750M is $0.56 \text{ Å pixel}^{-1}$ ($26 \text{ km s}^{-1} \text{ pixel}^{-1}$), so that no overlap of the monochromatic images occurred in the [S II] lines, nor between [N II] 6548 Å and H α , for nebulae less than $\approx 1''.4$ in diameter. Some of the nebulae are larger than this, and for these cases the continuum images were used to help distinguish the spatial features from velocity structure. (The overlapping lines for a few of the nebulae do not affect the measurements and classifications presented in this paper.) The G430M spectra cover the wavelength range from 4818–5104 Å, and include emission from H β 4861 Å and [O III] 4959, 5007 Å. These lines provide the morphology at intermediate ionization, and can also be used to

infer the ionization structure within the nebulae. The mean dispersion of $0.28 \text{ \AA pixel}^{-1}$ ($17 \text{ km s}^{-1} \text{ pixel}^{-1}$) means that the internal velocity structure of some of the nebulae could have been resolved, though this did not impede our ability to assign a morphological classification.

2.3. Calibration

The images and slit-less spectrograms were calibrated with the standard STIS calibration pipeline, version 2.3, released 1999 October (see Hodge, et al. 1998b). Processing in all cases included basic two-dimensional reductions, as described in Hodge, et al. (1998a), including corrections for bias and dark current, flat-fielding, and the combination of the paired exposures to remove cosmic rays. Special care was taken with the correction for the dark current because the temporal variation, which is related to the constant exposure of the CCD to high energy charged particles, is quite significant on a timescale of days. The calibration reference files for the dark correction are available from the *HST* archive approximately monthly, although individual dark frames are obtained on a daily basis. We down-loaded a script from the ST ScI Web site which enabled us to combine the so-called “weekly” dark reference files with ~ 5 individual dark frames that were obtained within a few days of each observation. The script corrects new hot pixels that deviate by more than 5-sigma from the weekly dark by using the median of the daily dark frames at that location. The resulting images are significantly improved compared to those processed without the constructed dark frame. However, it is apparent that a number of hot pixels are not corrected, or are not adequately corrected, by this procedure, which compromises the photometric accuracy on small spatial scales. Fortunately, none of the measurements or assessments offered in this paper are affected in a significant way by the imperfect dark correction.

3. Dimensions and Morphology

The broad-band and [O III] 5007Å images for the target nebulae (apart from three: see § 3.1 below) are presented in Figures 1 through 11; the broad-band data are rendered as grey-scale images, and the [O III] images are rendered as con-

tour plots. The grey-scale mapping is either the log or the square-root of the image intensity, in order to bring out the often faint structural features. The plots show contours on a linear scale, with 10% intensity intervals, to illustrate the structural features that are most relevant for the morphological classification.

We classified the morphologies in our sample from the [O III] 5007 Å monochromatic images in the G430M spectra (although we were guided by the H α and [N II] 6548 Å images), using a classification scheme similar to Manchado, et al. (1996). This classification scheme was recently extended (Górny, Stasińska, & Tylenda 1997; Stanghellini, et al. 1999) to recognize explicitly the bipolar core (BC) nebulae that show distinct hemispheres of emission in the nebular core. Usually, but not always, such nebulae were classified as “Rs” or (more often) “Es” in the Manchado, et al. (1996) scheme, meaning that such nebulae have round or elliptical outer contours, but have internal structure. Our designation of BC indicates the presence of a bi-nebulous structure with an intensity contrast of $\gtrsim 20\%$. When present, such structure is in our view the more important morphological feature, in that these nebulae are more closely connected to pure bipolar (B) PNe than either R or E (see § 4, below). Support for this view also comes from L. Stanghellini (2000, in preparation), who found that the BC PNe in the Galaxy have a disk scale height that is much more similar to that of B than to E or R nebulae. Our distinction between E and R was based on whether the major axis of the 10% intensity contour exceeded the minor axis by more than 10%.

Usually the morphological class we assigned on the basis of structures evident in the [O III] image would not have been different had we instead used another, lower-ionization line such as [N II] 6583 Å. But in four cases (15% of the resolved nebulae) the classification might have changed: we identify these cases in the notes on individual nebulae, below. Table 2 gives our classifications and the nebular dimensions. The nebular dimensions were measured with respect to the 10% intensity contour of the outermost structure, and are presented in column 5 of the table. We also measured the formal photometric radii, according to the method described by Stanghellini, et al. (1999). This measurement gives an objective measurement of neb-

ular angular size which is insensitive to the S/N ratio of the image, and is useful for evolution studies. It corresponds to the size of a circular aperture that contains 85% of the flux in [O III] 5007 Å, and is given in column 4 of the table.

3.1. Individual Nebulae

We describe in this section the morphological details for each nebula listed in Table 2.

J 41: This nebula has two distinct shells with elliptical outer contours, and an inner core that is bipolar in the light of H α . The classification was based solely on the H α image, since no other emission lines were available. The central star is easily detected.

SMP 4: This elliptical PN has a faint, elliptical outer shell: it could be classified as E/AH following the Stanghellini & Pasquali (1995) classification scheme for multiple shell PNe. The central star is easily visible in the continuum image.

SMP 9: This nebula has a barrel shape, but the outer contour is elliptical. In the emission line images there is a marginal detection of a central equatorial enhancement (i.e., a ring). No central star is detected.

SMP 10: This spiral-shaped object has a classic point-symmetric morphology that is strikingly like that of a spiral galaxy. Although this morphology is unusual for a PN (and it is the only such PN known in the LMC), there is a Galactic PN (“GPN”), K4–55 (Manchado, et al. 1996) that looks very similar. SMP 10 could also be an *incomplete bipolar*, seen face on (see NGC 6309 in the catalogs by Balick 1987 and Schwarz, Corradi, & Melnick 1992). In SMP 10 two limbs, or arms, project obliquely on opposite side of an elliptical, almost round main body: one east of north, and the other west of south. In the [N II] images they measure about 0''1 at maximum thickness and 1''3 in extent. The nebula is of moderate overall ionization, but the *arms* include a region of distinctly lower ionization: these features are readily apparent on the [N II] 6548,83 Å lines but are less distinct in the H α image, and even less so in the [O III] images. The presence of these features is reminiscent of the Galactic PN NGC 6543, though of course the spatial resolution is insufficient to determine whether a jet from the central star is present and related to the low ionization emission

regions. The central star is easily visible in the continuum image.

SMP 13: This nebula has a round outer contour, with a bipolar, if somewhat patchy, inner core. There is little if any stratification in the ionization. The central star is easily detected.

SMP 16: This is a bipolar planetary nebula with thick ring and a classic “butterfly” shape. Knots of emission are apparent along the ring in the [N II] images, but are less distinct in the H α and [O III] images. The ionization varies throughout the nebula: it is relatively high in the ring and the “wings” of the butterfly shape, but drops considerably near the outer edges of the wings. The nebula resembles the GPN NGC 2346. The central star is not visible through the ring.

SMP 18: The uncertain classification of this PN is a result of the contrast between its elliptical (possibly with a multiple shell) appearance in the continuum image, and either a slight asymmetry or a small central cavity the H α and [O III] images. The central star may be marginally detected.

SMP 19: This PN has an elliptical outer contour, but a clearly bipolar core. The ring-like structure is most apparent in the [N II] images. The central star is marginally detected.

SMP 25: This small PN has an elliptical outer contour, and a Gaussian intensity profile. The central star is easily detected.

SMP 27: The core of this object has the same quadrupolar morphology in all detected lines, including the broad-band image. Two extended nebular features are evident, though faint, in H α , [O III] 5007, and the broad-band image. The outermost is an arc approximately 6''25 to the NW, which is directed inward (to the CS), with a curvature that is somewhat larger than that of a circle centered on the CS. This arc is approximately 7''5 long and 0''5 wide, and has a surface brightness ~ 10 times fainter than the central nebula. The other feature is a blob centered approximately 4''8 to the north, with dimensions 2''7 x 1''0, with a similar surface brightness to the arc. The blob is roughly aligned with the major axis of symmetry of the inner nebula.

The central (bright) region of this object is very highly ionized: there is no detection of [S II], [O I], and only very weak [N II]. On the other hand, [O III] 5007, 4959 are very strong relative

to $H\beta$, and He I 6678 is easily detected. A ratio of the [O III] 5007 to $H\alpha$ images shows a relatively uniform inner structure, though the ratio falls to roughly one-third of the core value in the outer structures. Though the ionization apparently declines with distance from the CS, the ratio could conceivably be affected by a higher electron temperature or, alternatively, a higher O^{++} abundance in the inner region; long-slit spectroscopy with STIS can resolve this question.

It is very tempting to associate the outer features with the central PN, especially since it is otherwise not obvious how this gas is ionized. The features are not quite circularly symmetric, though this is not unusual for GPNe. Also, the outer features are at the limit of detection on these images, and other features may lurk beneath the noise. The central star is bright, and easily detected in the continuum image and in the dispersed images. SMP 27 has a measured expansion velocity of 33 km s^{-1} (Dopita, et al. 1988). If this velocity were constant throughout the life (and spatial extent) of the nebula, the implied dynamical age is 3500 yr for the inner region, and $\sim 45,400$ yr for the outer arc. A plausible explanation for the presence of the outer ionized structure is that the ionization front from the inner nebula has encountered remnant gas from the AGB wind that preceded the formation of the inner nebula, and the subsequent evolution of the CS to high temperature. The near-alignment of the ionized blob and the symmetry axis of the inner nebula suggests a kinematic connection to an asymmetric ejection from the CS.

SMP 28: At the first sight, this PN can be considered *bi-nebulous* (Greig 1972), in that its main shape comprises two distinct blobs. Closer inspection of the $H\alpha$ and [N II] images reveals three roughly co-aligned blobs, separated by $0''.2$. The central blob is the brightest, and corresponds to the position of the central star, which is apparent on the continuum image. Two faint, thin arms are evident in the light of [N II] that extend obliquely from opposite sides of the central blob, which may be similar to the arms seen in SMP 10.

SMP 30: This object is morphologically similar to NGC 6853 in the Galaxy. Although this PN is clearly asymmetric, it is difficult to say for certain whether the morphology is bipolar or quadrupolar. The ionization structure is relatively

complex: the ionization in general declines from center to the periphery, but there are tight knots of [N II] bright material at the ends of an equatorial axis that are rather more diffuse in the light of [O III]. A very faint star is detected close to the center of symmetry, which is probably the central star.

SMP 31: This PN is barely resolved; the classification as “R” is therefore uncertain. No central star is apparent.

SMP 34: Although this PN appears round in the continuum image as well as the $H\alpha$ and [O III] images; there is a hint of bipolar structure in the light of [N II]. The central star is detected.

SMP 46: This PN is ring-like in appearance, with a bright knot on the southwestern edge. No central star is detected.

SMP 53: This elliptical, barrel shaped PN does not clearly show a bipolar core. Nonetheless, a ring of emission is very clear in the light of a [N II] (and to some extent in $H\alpha$), thus we classify it BC. No central star is detected.

SMP 58: This PN is barely resolved; the classification as “R” is therefore uncertain. The central star is probably detected. We do not show this object in the figures, since there are no significant morphological features or nearby field stars of comparable brightness.

SMP 59: This object has quadrupolar morphology in all detected lines, including the broadband image. It shows a lot of internal structure, with a very knotty major axis, and a fainter minor axis that is not orthogonal (in the plane of the sky) to the major axis. The ionization structure generally follows the spatial structure, except that the knots of emission are spatially more confined in the light of [N II]. The bright central star is easily detected in both the continuum and the dispersed images.

SMP 65: This PN would be a classic round PN were it not that the core of the $H\alpha + [O III]$ emission is slightly displaced $\sim 0''.1$ north of the CS. This object also has a faint, outer halo. The ionization is spatially fairly uniform, and relatively high, with no [N II] or other low-ionization species present in the spectrum. No central star is detected.

SMP 71: This PN is elliptical in every contour of constant intensity, but the major axis of the

ellipse in the inner (bright) region is orthogonal to that of the outermost contour. The central star is not detected.

SMP 78: This object shows a barrel-shaped morphology very similar to that of SMP 53, except that the bipolar core is more evident. There is little ionization stratification, and no central star is detected.

SMP 79: This PN has an elliptical outer contour, with a bipolar core. This is the physically smallest BC nebula in the sample, with a radius of 0.05 pc, and a dynamical age of ~ 1400 yr, assuming a constant expansion velocity of 37 km s^{-1} (Dopita, et al. 1988). The central star is not detected.

SMP 80: This is a round PN in continuum light, and in the light of $H\alpha$ and in the [O III] lines. However, the [N II] lines reveal an inner ring or bipolar shell that is $\approx 0''.4$ in diameter.

SMP 81: This PN is barely resolved; the classification as “R” is therefore uncertain. The central star is detected. We do not show this object in the figures, since there are no significant morphological features or nearby field stars of comparable brightness.

SMP 93: This object is perhaps the most visually striking of the PN images presented here; we refer to it as the “monkey head” nebula. The morphology in continuum light and in all the detected emission lines shows a set of at least three asymmetric, interconnected rings. The strong [N II] lines show faint emission “bubbles” beyond the outermost rings, along the long axis of symmetry. With a maximum extent of $6''.4$, or 1.57 pc, this object ranks with the very largest PNe known in the Galaxy. The morphology is closely analogous to the GPN M2–53. No central star is apparent.

SMP 94: This object is not resolved (and hence is not shown in the figures). The dispersed images show a double-peaked velocity structure, with a width of $\sim 200 \text{ km/s}$. The ionization is fairly high, but peculiar, with prominent $H\alpha$, rather weak [O III] lines, and broad He II 6830 Å emission as well. These features suggests that this object may not be a PN, but could be a symbiotic star, as suggested by Dopita, et al. (1988).

SMP 95: This PN has an elliptical outer contour, but a clearly bipolar core, with faint ansae extending from the ends of the major axis of sym-

metry. This object shows moderate ionization, with prominent [O III] lines, but relatively strong [O I], [N II], and [S II] lines as well. No central star is detected.

SMP 100: This is a most interesting PN, with rather complex morphological features and ionization structure. This object has an elliptical outer contour and a bipolar (or possibly quadrupolar) core denoted by bright lobes at either end of the minor axis, though the lobe to the NW is brighter by nearly half and much more spatially extended. The structure in the [O III] lines is similar to that in $H\alpha$, except that the brightness contrast in the lobes is much higher in [O III]. The low-ionization [N II] lines, on the other hand, are only detected in knots that define a ring, with the strongest knots lying just outside the ends of the [O III] emission lobes. The central star is somewhat faint, but is easily detected.

SMP 102: This object is a round PN, with many emission knots surrounding a central cavity; it may have a bipolar core. The ionization is relatively high, with no emission detected in the [N II] lines *except* in the bright knot lying to the SW of the moderately bright central star.

4. Discussion

4.1. The Full Sample

With this dataset, together with the 31 resolved LMC PNe for which monochromatic images exist in the *HST* archive, we can for the first time compare the incidence of PNe among morphological types between the LMC and the Galaxy, and search for evidence of temporal evolution among morphological types. For this purpose we adopted the dimensions and morphological data from Stanghellini, et al. (1999). We also retrieved archival *HST*/WFPC2 images of 14 additional LMC PNe from the GO program 6407 (PI: M. Dopita). These images were obtained with narrow-band filters centered on [O III] 5007 Å and $H\alpha$ 6563 Å (though in the latter case there is some contamination from [N II] 6548 Å, which is of no consequence here). Our dimensional measurements and morphological classifications, which were performed exactly as for the STIS data presented above, are independent of the quality of the calibration. However, the derivation of the mean surface brightness (discussed below)

does require a good calibration, so we re-calibrated the WFPC2 data using the standard pipeline, and performed cosmic-ray rejection when more than one frame was available. The dimensions and our morphological classifications for these objects are given in Table 3.

4.2. Morphology and Nebular Evolution

In Table 4 we compare the relative number of PNe in each morphological class from the combined LMC sample with that in the Galaxy, based on our classification of the PNe in the sample defined by Manchado, et al. (2000). We re-classified all of these nebulae because the BC class was not recognized as important in itself when these catalogs were published, and because we were interested to see whether our classifications agreed those of other experts in the field. Our BC nebulae corresponded to a subset of what had been classified as E or R in the earlier catalogs—and very often these nebulae were given a sub-class of “s” to denote some degree of apparent structure. Apart from this distinction the disagreements were rare. For the comparison between the LMC and the Galaxy, the B, BC, and Q, types were combined to form a single “asymmetric” class of nebulae. This comparison is important because bipolarity has been shown to be an indication of Population I ancestry for PNe in the Galaxy, and recently this relationship has been extended to the LMC by Stanghellini, et al. (2000). Though the number of classified nebulae in the LMC (59) is $\sim 1/5$ the number in the Galactic sample, the fractions of elliptical vs. asymmetric nebulae are quite different between the LMC and the Galaxy. Taken at face value, this result would imply that a much larger fraction of the PNe in the LMC were produced by a younger Population of stars than in the Galaxy. If so, the most direct interpretation would be that the star formation history of the LMC PNe progenitors is very different than that of the Galaxy (averaged over the volume defined by the Galactic PN sample). While there is evidence to support a burst of star formation occurring in the LMC within the last 4 Gyr (Grebel 1998), it may well be that some, or perhaps most, of the discrepancy between PN morphological classes can be attributed to selection effects in either PN sample.

We next explore the question of temporal evolution of nebular morphology by examining it in the

context of the change in nebular surface brightness with nebular size. All of the nebulae are resolved, though three are smaller than $0''.30$ (6 pixels) in diameter. We present the relationship in Figure 12, where the various morphological types are mapped to symbols according to the legend. For this purpose, we actually derive the mean surface brightness in the $[\text{O III}] 5007\text{\AA}$ line within the photometric radius, corrected for interstellar extinction according to the formula:

$$I_{corr} = I_{obs} \times 10^{c*(1+f_\lambda)}$$

where c , the logarithmic extinction at $H\beta$, is taken from Meatheringham & Dopita (1991a,b) and f_λ , the extinction law from Howarth (1983) for the LMC, is approximately 0.02 at 5007\AA . Since this sample is drawn entirely from the LMC, the radius is linearly proportional to the physical size of the nebula, which is also a rough indicator of nebular age (but see § 4.3 below). The dotted line in the figure corresponds to a decline in nebular surface brightness proportional to R^{-3} , which is roughly consistent with the data. The actual change in surface brightness of an evolving PN must relate in a fairly complex way to the expansion of the nebula, the change in ionization, temperature and density of the gas, and the simultaneous and potentially very large changes in the temperature and luminosity of the central star as it evolves during the PN lifetime. That this relationship could be so simply characterized (albeit with large deviations) is interesting, and may help constrain evolutionary models.

The figure shows that ten of the eleven angularly smallest nebulae ($0''.13 \leq R_{Phot} \leq 0''.26$) are round or elliptical. In this size regime most of the nebulae are well resolved (i.e., exceed in size a STIS CCD spatial resolution element of 2 pixels), and the detected signal per pixel is very high (usually $> 10^4$ counts pixel $^{-1}$, and $> 10^5$ counts in total). However, three of the nebulae have radii of $\leq 0''.15$; the morphological classification in these cases is less certain because faint structural details may not be resolved. The lack of asymmetric nebulae at small sizes could be interpreted as an evolutionary effect: that is, any initial asymmetry in the gas distribution and velocity field of R or E nebulae may not have had time to manifest itself in the morphology, while extreme B nebulae (the progeny of the most massive and luminous central

stars) may evolve so quickly through this phase that they are unlikely to be detected. As we will show in the next subsection, the asymmetric nebulae in this sample have higher mean expansion velocities. But we cannot rule out the possibility that observational selection is largely responsible for the disproportionate fraction of R+E nebulae at small size, mostly because the catalogs from which we selected our sample contain PNe that are relatively bright in [O III] 4959, 5007Å, the presence of which is often used as a criterion for classification as a PN. Certainly the small number statistics in this size regime makes firm conclusions about evolutionary effects for small PNe difficult. In any case, the onset of asymmetric features is known to appear in very young Galactic PNe (e.g., M 2-9 and CRL 2688), and even SMP 74 in the LMC is probably younger than 2000 yr. This suggests that the gross features of the nebular morphology are well connected to PN formation. What is more clear in our sample is the segregation of bipolar core PNe (between $0''.30 \leq R_{Phot} \leq 0''.70$), which have a round or elliptical outer contour, and pure bipolar nebulae ($> 0''.70$, or > 0.18 pc). This suggests that the bi-polarity may become the dominant morphological feature during the lifetime of BC nebulae, perhaps through subsequent shaping by the radiation field and wind from the central star (Balick 1987). This result, when combined with the identification of BC with B as the products of a younger stellar population (Stanghellini, et al. 2000), lends support to the identification of the BC class as a physically important morphological feature.

4.3. Nebular Expansion

We alluded above to the connection between the physical size of the PN and its age, i.e., the time elapsed since the visible PN shell was ejected from its progenitor. The “dynamical” age, the ratio of the physical size to the current expansion velocity, has been used for this purpose under the assumption that the expansion has been constant throughout the life of the nebula. The validity of this assumption has been questioned by many, and some (e.g. Dopita, et al. 1987; Dopita & Meatheringham 1990; Dopita, et al. 1996; Vassiliadis, et al. 1998) have argued that the nebular shell experiences acceleration during the transition of the CS to high temperature at constant luminosity. We

explore this point in Fig. 13, where we show the variation of nebular expansion velocity with physical radius for this LMC sample. The physical radius was derived from our data by scaling the photometric radius by $0.245 \text{ pc arcsec}^{-1}$; the velocities, derived from the [O III] 5007 Å line, were taken from Dopita, et al. (1988) and corrected according to Stanghellini, et al. (1999) (i.e., those derived by measuring the width of single line profile were reduced by a factor of 1.82). The most striking feature of this plot is that, for nebulae smaller than ~ 0.1 pc, the expansion velocities deviate, and are generally less than, the mean of $\sim 20 \text{ km s}^{-1}$. The significant differences between this plot and that in Dopita & Meatheringham (1990, Fig. 4) are that the nebular radii are much more accurate, and that the morphological types are known. All of the PNe in this range are of type R or E, though the types of the three smallest nebulae are less certain (see § 4.2). A possible interpretation is that nebular shells experience an acceleration from the central star until they reach a critical size, by which time the acceleration becomes negligible either because of geometrical dilution of the shell or because the central star luminosity has substantially declined. Which effect applies would depend upon the relative rate of evolution of the shell vs. the central star: the less massive CSs have lower maximum luminosities, and therefore might be expected to provide less acceleration. At the other extreme, another possibility is that acceleration of the shells is nearly zero in these PNe (i.e., those larger than 0.03 pc), but that some nebulae (mostly of type R or E, evidently) expand very slowly. In this case, the nebulae would have to fade below the detection limit before they reach $\sim 0''.1$ in size.

We believe it is difficult to draw firm conclusions about shell accelerations, and therefore about nebular dynamical ages, based upon the available velocity data. The spectra of the [O III] 5007 Å profiles were obtained at $\approx 12 \text{ km s}^{-1}$ resolution (Dopita, et al. 1988), so that in a number of cases the correction for the instrumental profile was comparable to or exceeded the measurement (see the dotted line in Fig. 13). Ignoring these points significantly weakens the case for acceleration in this size regime. More importantly, the spectrograms did not resolve the nebulae spatially, so that high velocity components, when de-

tected, cannot be associated directly with common morphological details seen in these or other nebulae, such as shells, rings, FLIERS, or jets. That is, at least for some nebulae, it is not clear whether the expansion velocity measured from this one moderate-ionization line is representative of the nebular expansion as a whole. To illustrate the point, nebulae in which multiple velocity components were detected are connected in the Figure with symbols at the extrema of the velocity range. Detailed interpretation of complex velocity structures in PNe, such as that published by Guerrero, et al. (2000) for NGC 6891, is very important for establishing the kinematics of the expanding nebula. We believe it is important to obtain spatially resolved, high resolution spectroscopy of the LMC PNe to relate reliably the expansion velocities to nebular dynamical ages.

4.4. Caveats and Selection Effects

Although we believe the morphology of PNe in the LMC reveals an important clue about the Population of the progenitors, we must be mindful of selection effects that may affect our interpretation. As we described in § 2.1, our sample was drawn from surveys that are known to be incomplete, either in depth or in spatial coverage (Jacoby 1980; Leisy, et al. 1997). Since few known LMC PNe are resolvable from the ground, the spectroscopic criteria for identification as PNe often includes bright [O III] emission, which selects against the youngest PNe (where the ionization has not yet reached the point where significant O^{+2} has been produced), and the very oldest PNe (where the ionization has declined because of the dimming and dilution of the CS radiation field). Few of these surveys probe very deeply, and in any case our program did not include more than a very few PNe that were moderately faint (in either or both of $H\alpha$ and [O III]). Figure 12 shows that, to first order, excluding the faintest PNe also excludes the dynamically oldest PNe. The Galactic sample may also suffer from selection bias. For instance, the asymmetric PNe may be under-represented in the Galactic sample since they are more closely confined to the disk, and hence suffer more attenuation (on average) from interstellar dust, which would select against their discovery.

Finally, the spatial coverage of the discovery surveys does not extend to the faintest regions of

the LMC (Morgan 1994), which excludes PNe that could be the progeny of a much older population of stars. Fig. 14 shows the spatial distribution of this sample of PNe, relative to the LMC bar, coded by morphological type. Most of these PNe lie within $\sim 2^\circ$ of the bar, which is consistent with the optical continuum distribution of light from stars. We know of no particular segregation of population types (other than young stars in H II regions) in the LMC, though some studies suggest that tidal interactions with the Galaxy greatly perturb the orbits of moderate to old stars (e.g., Weinberg 2000). Certainly the spatial distribution of nebular morphologies in Fig. 14 shows no particular segregation within the LMC, other than that there are more PNe of all types in the bar. While this distribution is consistent with that for the older stellar Populations, it is probably fortuitous given the selection effects mentioned above.

5. Conclusion and Future Work

We have used the *HST* and STIS in slit-less mode in a campaign to obtain monochromatic images of a large sample of Magellanic Cloud PNe in several important emission lines. The set of LMC PNe presented here display a wide variety of morphological features, including examples of the rare Quadrupolar and Point-Symmetric classes. We argue that bipolar core PNe are a variant of, and sometimes an evolutionary precursor to, the pure bipolar class. Such a finding is consistent with published evidence that BC nebulae are closely related to type B PNe (and are not similar to E or R PNe) in chemical abundances, progenitor Population type, and (for Galactic PNe) disk scale height. It is important that future studies compare the relative ages of BC and B nebulae through other means, such as the evolutionary state of the central stars, to confirm our suggestion that some or most BC nebulae evolve to B. It is also very important to increase the sample size of observed B and BC nebulae in the Magellanic Clouds, and to obtain high resolution, spatially resolved spectrograms to interpret properly the kinematics of the expanding shell(s), and therefore the nebular dynamical ages.

The nebulae presented here roughly double the number of LMC PNe that have been imaged with *HST*, and in that combined dataset we find a

larger fraction of asymmetric PNe in the LMC than in the Galaxy. This result either suggests a difference in the stellar Population types and/or star formation history between the LMC and the Galaxy, or it shows us the extent to which selection effects operate in studies of PN morphology. We also find evidence for evolution in nebular morphology, but the extent to which it is determined by PN formation processes vs. subsequent star + wind interactions is less clear: this question must be pursued by including younger PNe in the study. In any event, the smallest (and presumably the youngest) BC nebula in our sample is ≈ 0.05 pc in radius, implying a rough dynamical age of ~ 1400 yr, which shows that the onset of asymmetrical features can occur very early in the PN lifetime. The implication is that, for at least some nebulae, the gross morphological features are more closely tied to PN formation, and that subsequent shaping of the expanding envelope by the radiation field and wind from the central star plays the lesser role of amplifying these features. This conclusion is consistent with data from young Galactic PNe, except that for LMC PNe the determination of the size of the ionized nebula and the dynamical age are far more secure.

We will present measurements and analysis of the nebular plasma diagnostics and chemical abundances in a future paper. We will also present continuum magnitudes for the detected central stars, which will allow us to determine their evolutionary state. These analyses form a key part of our intended research in this area, where we will be able to analyze the co-evolution of the PNe and their central stars without the debilitating uncertainties of the Galactic PN distance scale. It will also give us a much more accurate picture of the chemical yields of PNe in the LMC. We plan to extend this work to SMC PNe, where the lower metallicity environment should yield a difference in the morphological types, and perhaps also a difference in important aspects of the stellar and nebular evolution.

Support for this work was provided by NASA through grant number GO-08271.01-97A from Space Telescope Science Institute, which is operated by the Association of Universities for Research in Astronomy, Incorporated, under NASA contract NAS5-26555. We are grateful to an

anonymous referee, whose comments helped us to improve this paper.

REFERENCES

- Acker, A., Gleizes, F., Chopinet, M., Marcout, J., Ochsenbein, F., & Roques, J. 1982, Catalogue of the Central Stars of True and Possible Planetary Nebulae (Strasbourg, Fr: Obs. de Strasbourg)
- Balick, B. 1987, *AJ*, 94, 671
- Blades, J. C., et al. 1992, *ApJ*, 398, L44
- Corradi, R. L. M., & Schwarz, H. E. 1995, *A&A*, 293, 871
- Dopita, M. A., & Meatheringham, S. J. 1990, *ApJ*, 357, 140
- Dopita, M. A., Meatheringham, S. J., Wood, P. R., Webster, B. L., Morgan, D. H., & Ford, H. C. 1987, *ApJ*, 315, L107
- Dopita, M. A., Meatheringham, S. J., Webster, B. L., & Ford, H. C. 1988, *ApJ*, 327, 639
- Dopita, M. A., et al. 1996, *ApJ*, 460, 320
- Górny, S. K., Schwarz, H. E., Corradi, R. L. M., & Van Winckel, H. 1999, *A&AS*, 136, 145
- Górny, S. K., Stasińska, G., & Tylenda, R. 1997, *A&A*, 318, 256
- Greig, W. E. 1972, *A&A*, 18, 70
- Grebel, E. K. 1998, in Proc. of the XVII-Ith Moriond Conf. on “Dwarf Galaxies and Cosmology,” *Les Arcs*, eds. T. X. Thuan, C. Balkowski, V. Cayatte, J. Tran.
- Guerrero, M. A., Miranda, L. F., Manchado, A., & Vázquez, R. 2000, *MNRAS*, 313, 1
- Hodge, P. E., et al. 1998a, STIS Instrument Science Report 98–10 (Baltimore: ST ScI)
- Hodge, P. E., et al. 1998b, STIS Instrument Science Report 98–26 (Baltimore: ST ScI)
- Howarth, I. D. 1983, *MNRAS*, 203, 301
- Jacoby, G. H. 1980, *ApJS*, 42, 1
- Iben, I., Jr., Kaler, J. B., Truran, J. W., & Renzini, A. 1983, *ApJ*, 264, 605
- Kaler, J. B. 1982, *IAU Symp.* 83, ed. D. R. Flower, (Dordrecht: Reidel), 245
- Kimble, R. A., et al. 1998, *ApJ*, 492, L83
- Leisy, P., Dennefeld, M., Alard, C. & Guibert, J. 1997, *A&AS*, 121, 407
- Manchado, A., Guerrero, M., Stanghellini, L., & Serra-Ricart, M. 1996, The IAC Morphological Catalog of Northern Galactic Planetary Nebulae (Tenerife: IAC)
- Manchado, A., Villaver, E., Stanghellini, L., & Guerrero, M. 2000, in *ASP Conf. Ser.* 199, *Asymmetrical Planetary Nebulae II: from Origins to Microstructures*, eds. J. H. Kastner, N. Soker, & S. A. Rappaport, (San Francisco: ASP), 17
- Meatheringham, S. J., & Dopita, M. A. 1991a, *ApJS*, 75, 407
- . 1991b, *ApJS*, 76, 1085
- Morgan, D. H. 1994, *A&AS*, 103, 235
- Peimbert, M. 1978, *IAU Symp.* 76, ed. Y. Terzian, (Dordrecht: Reidel), 215
- Peimbert, M., & Torres-Peimbert, S. 1982, *IAU Symp.* 83, ed. D. R. Flower, (Dordrecht: Reidel), 233
- Sanduleak, N., MacConnell, D. J., & Phillip, A. G. D. 1978, *PASP*, 90, 621
- Schwarz, H. E., Corradi, R. L. M., & Melnick, J. 1992, *A&AS*, 96, 23
- Stanghellini, L., Blades, J. C., Osmer, S. J., Barlow, M. J., & Liu, X.-W. 1999, *ApJ*, 510, 687
- Stanghellini, L., Corradi, R. L. M., & Schwarz, H. E. 1993, *A&A*, 279, 521
- Stanghellini, L., & Pasquali, A. 1995, *ApJ*, 452, 286
- Stanghellini, L., Shaw, R. A., Balick, B., & Blades, J. C. 2000, *ApJ*, 534, L167
- Vassiliadis, E., Dopita, M. A., Meatheringham, S. J., Bohlin, R. C., Ford, H. C., Harrington, J. P., Wood, P. R., Stecher, T. P., & Maran, S.-P. 1998, *ApJ*, 503, 253
- Weinberg, M. 2000, *ApJ*, submitted
- Woodgate, B. E., et al. 1998, *PASP*, 110, 1183

Figure Captions

Fig. 1.— Images (*left*) and contour maps (*right*) of the LMC PNe J 41 (*upper*), SMP 4 (*middle*), and SMP 9 (*lower*). The images were obtained using the clear (50CCD) bandpass, and are $3''$ on a side, with a log intensity stretch. The contour maps are from the G430M slit-less spectra, in the monochromatic light of [O III] 5007\AA (except for J 41, which is in the light of $H\alpha$, taken from the G750M spectrum). The contours are drawn at roughly 10% intensity intervals. The orientation for each image is indicated on the figure, with north lying in the direction of the arrow, and east to the left.

Fig. 2.— Same as Fig. 1 for the nebulae: SMP 10 (*upper*), and SMP 16 (*lower*). These images are $4''$ on a side, but are on the same scale.

Fig. 3.— Same as Fig. 1 for the nebulae SMP 13 (*upper*), SMP 18 (*middle*), and SMP 19 (*lower*).

Fig. 4.— Same as Fig. 1 for the nebulae SMP 25 (*upper*), SMP 28 (*middle*), and SMP 30 (*lower*).

Fig. 5.— Same as Fig. 1 for the inner (*upper*) and outer (*lower*) portions of the nebula SMP 27. The outer image is $9''$ by $12''$ and is presented at half the scale of the other images.

Fig. 6.— Same as Fig. 1 for the nebulae SMP 31 (*upper*), SMP 34 (*middle*), and SMP 46 (*lower*).

Fig. 7.— Same as Fig. 1 for the nebulae SMP 53 (*upper*), SMP 65 (*middle*), and SMP 71 (*lower*).

Fig. 8.— Same as Fig. 1 for the nebula SMP 59, except that the contour map is from the broadband (50CCD) image and the contours are evenly spaced in the square-root of the image intensity. This image is $5''$ square.

Fig. 9.— Same as Fig. 1 for the nebulae SMP 78 (*upper*), SMP 79 (*middle*), and SMP 80 (*lower*).

Fig. 10.— Same as Fig. 1 for the nebula SMP 93, except that the contour map is from the broadband (50CCD) image. This image is $6''$ by $8''$ and is at 75% of the scale of the other images.

Fig. 11.— Same as Fig. 1 for the nebulae SMP 95 (*upper*), SMP 100 (*middle*), and SMP 102 (*lower*).

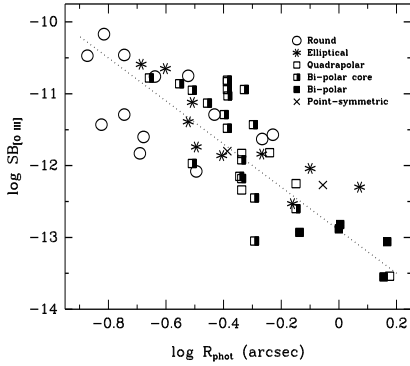


Fig. 12.— The decline of surface brightness, in the light of $[O III] 5007\text{\AA}$, with nebular (photometric) radius is consistent with an R^{-3} power law (*dotted line*). The various morphological types are represented by different symbols, as shown in the legend.

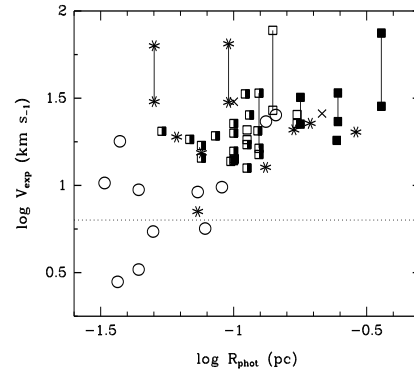


Fig. 13.— Nebular expansion velocity (adapted from Dopita, et al. 1988, see text) as a function of nebular physical radius. Greater uncertainty likely applies to values of V_{exp} for which the correction for the instrumental resolution (*dotted line*) is large. Nebulae in which multiple expansion components were detected are shown at the extrema of the published velocity range, and are connected with vertical lines. Symbols as in Fig 12.

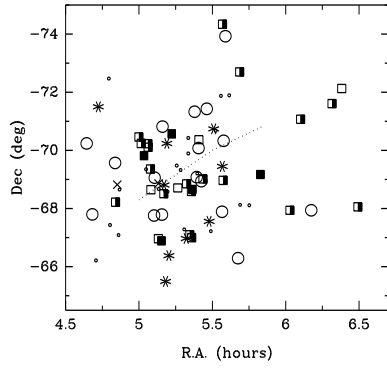


Fig. 14.— Surface distribution of PNe in the LMC that have been imaged with *HST*. Symbols as in Fig 12, except that small circles denote PNe in our SNAP program that have not yet been observed. The approximate location of the axis of the LMC bar is shown (*dotted line*).

TABLE 1
OBSERVING LOG FOR LMC PLANETARY NEBULAE

Nebula	Date	Dataset	Disperser	T_{Exp} (s)	N_{Exp}
J 41	1999-Sep-02	O5BM50010	MIRVIS	300	2
		O5BM50020	G750M	1780	2
SMP 4	1999-Aug-20	O5BM22010	MIRVIS	120	2
		O5BM22020	G750M	730	2
		O5BM22QHQ	G750M	90	1
SMP 9	1999-Aug-12	O5BM22030	G430M	280	2
		O5BM23010	MIRVIS	120	2
		O5BM23020	G750M	550	2
		O5BM23LRQ	G750M	70	1
SMP 10	1999-Sep-28	O5BM23030	G430M	300	2
		O5BM24010	MIRVIS	120	2
		O5BM24020	G750M	360	2
SMP 13	1999-Aug-15	O5BM24D2Q	G750M	45	1
		O5BM24030	G430M	360	2
		O5BM04010	MIRVIS	120	2
		O5BM04BBQ	MIRVIS	15	1
SMP 16	1999-Aug-09	O5BM04020	G750M	170	2
		O5BM04BFQ	G750M	20	1
		O5BM04030	G430M	74	2
		O5BM27010	MIRVIS	300	2
SMP 18	1999-Aug-09	O5BM27020	G750M	1500	2
		O5BM27030	G430M	600	2
		O5BM29010	MIRVIS	120	2
SMP 19	1999-Aug-20	O5BM29020	G750M	580	2
		O5BM29DZQ	G750M	72	1
		O5BM29030	G430M	340	2
		O5BM05010	MIRVIS	120	2
		O5BM05QOQ	MIRVIS	15	1
SMP 25	1999-Aug-25	O5BM05020	G750M	136	2
		O5BM05QRQ	G750M	17	1
		O5BM05030	G430M	56	2
		O5BM06010	MIRVIS	120	2
		O5BM06FWQ	MIRVIS	15	1
		O5BM06030	G750M	300	2
SMP 27	1999-Jul-19	O5BM06020	G750M	60	2
		O5BM06FZQ	G750M	8	1
		O5BM06050	G430M	170	2
		O5BM06040	G430M	34	1
		O5BM30010	MIRVIS	120	2
		O5BM30020	G750M	630	2
		O5BM30DIQ	G750M	80	1
SMP 28	1999-Sep-12	O5BM30030	G430M	360	2
		O5BM31010	MIRVIS	120	2
		O5BM31020	G750M	560	2
SMP 30	1999-Aug-17	O5BM31LCQ	G750M	70	1
		O5BM31030	G430M	280	2
		O5BM32010	MIRVIS	120	2
		O5BM32020	G750M	700	2
SMP 31	1999-Aug-20	O5BM32HAQ	G750M	90	1
		O5BM32030	G430M	500	2
		O5BM33010	MIRVIS	120	2
SMP 34	1999-Sep-27	O5BM33020	G750M	210	2
		O5BM33Q9Q	G750M	26	1
		O5BM33030	G430M	1120	2
		O5BM08010	MIRVIS	120	2
SMP 46	1999-Sep-27	O5BM08020	G750M	200	2
		O5BM08CBQ	G750M	25	1
		O5BM08030	G430M	170	2
SMP 53	1999-Sep-18	O5BM36010	MIRVIS	120	2
		O5BM36020	G750M	1000	2
		O5BM36030	G430M	300	2
SMP 53	1999-Sep-18	O5BM11010	MIRVIS	120	2
		O5BM11ZAQ	MIRVIS	15	1
		O5BM11020	G750M	106	2
		O5BM11ZDQ	G750M	13	1
		O5BM11030	G430M	38	2

TABLE 1—*Continued*

Nebula	Date	Dataset	Disperser	T_{Exp} (s)	N_{Exp}
SMP 58	2000-Apr-29	O5BM12010	MIRVIS	120	2
		O5BM12CBQ	MIRVIS	15	1
		O5BM12030	G750M	380	2
		O5BM12020	G750M	76	2
		O5BM12CEQ	G750M	10	1
SMP 59	1999-Aug-02	O5BM12040	G430M	15	2
		O5BM39010	MIRVIS	120	2
		O5BM39020	G750M	880	2
SMP 65	1999-Aug-31	O5BM39030	G430M	480	2
		O5BM40010	MIRVIS	120	2
		O5BM40020	G750M	520	2
SMP 71	1999-Aug-25	O5BM40EOQ	G750M	65	1
		O5BM40030	G430M	420	2
		O5BM13010	MIRVIS	120	2
SMP 78	1999-Sep-28	O5BM13020	G750M	180	2
		O5BM13GCQ	G750M	22	1
		O5BM13030	G430M	70	2
		O5BM16010	MIRVIS	120	2
		O5BM16FJQ	MIRVIS	15	1
SMP 79	1999-Sep-28	O5BM16030	G750M	480	2
		O5BM16020	G750M	96	2
		O5BM16FMQ	G750M	12	1
		O5BM16040	G430M	90	2
		O5BM17010	MIRVIS	120	2
SMP 80	1999-Sep-29	O5BM17G6Q	MIRVIS	15	1
		O5BM17020	G750M	108	2
		O5BM17G9Q	G750M	13	1
		O5BM17030	G430M	120	2
		O5BM42010	MIRVIS	120	2
SMP 81	1999-Aug-10	O5BM42020	G750M	360	2
		O5BM42KTQ	G750M	45	1
		O5BM42030	G430M	280	2
		O5BM18010	MIRVIS	120	2
		O5BM18E6Q	MIRVIS	15	1
SMP 93	1999-Aug-11	O5BM18020	G750M	103	2
		O5BM18E9Q	G750M	13	1
		O5BM18030	G430M	33	2
		O5BM45010	MIRVIS	120	2
		O5BM45020	G750M	580	2
SMP 94	1999-Jul-31	O5BM45LFQ	G750M	72	1
		O5BM45030	G430M	530	2
		O5BM20010	MIRVIS	120	2
		O5BM20020	G750M	250	2
		O5BM20RAQ	G750M	31	1
SMP 95	1999-Jul-31	O5BM20030	G430M	90	2
		O5BM20040	G430M	480	2
		O5BM46010	MIRVIS	120	2
		O5BM46020	G750M	680	2
		O5BM46QRQ	G750M	85	1
SMP 100	1999-Aug-22	O5BM46030	G430M	300	2
		O5BM21010	MIRVIS	120	2
		O5BM21XTQ	MIRVIS	15	1
		O5BM21030	G750M	240	2
		O5BM21020	G750M	42	1
SMP 102	1999-Sep-29	O5BM21XWQ	G750M	5	2
		O5BM21040	G430M	150	2
		O5BM47010	MIRVIS	120	2
		O5BM47020	G750M	420	2
		O5BM47G1Q	G750M	52	1
		O5BM47030	G430M	240	2

TABLE 2
POSITIONS, DIMENSIONS AND MORPHOLOGIES OF LMC PLANETARY NEBULAE

Nebula	R.A. (J2000)	Dec. (J2000)	R_{Phot} (arcsec)	Dimensions (arcsec)	Morphological Classification	Notes
J 41	5:26:09.51	-69:00:58.4	0.51	inner: 0.69 x 0.62 outer: 1.17 x 1.10	E(bc)	No [O III] image available; faint outer halo
SMP 4	4:43:21.50	-71:30:09.5	0.69	1.21	E	Faint, round outer halo
SMP 9	4:50:24.71	-68:13:17.0	0.46	0.92 x 0.73	E(bc)	Barrel shape
SMP 10	4:51:08.90	-68:49:05.8	0.88	1.58 ^a	P	Spiral shape
SMP 13	5:00:00.07	-70:27:41.8	0.47	0.81	R(bc)	
SMP 16	5:02:01.91	-69:48:54.4	1.00	1.5 x 1.2	B	Butterfly shape
SMP 18	5:03:42.64	-70:06:47.8	0.51	0.69 x 0.64	R(bc?)	
SMP 19	5:03:41.30	-70:13:53.6	0.41	0.79 x 0.65	E(bc)	Ring
SMP 25	5:06:24.00	-69:03:19.2	0.23	0.42 x 0.39	R	
SMP 27	5:07:54.90	-66:57:46.1	0.46	0.76	Q	Outer arc and blob
SMP 28	5:07:57.61	-68:51:47.0	0.41	0.58 x 0.35	P	Outer contour non-E; arcs
SMP 30	5:09:10.61	-66:53:38.7	0.73	1.68 x 1.28	B?	Very irregular
SMP 31	5:09:20.23	-67:47:25.2	0.15	0.26	R?	
SMP 34	5:10:17.18	-68:48:23.0	0.32	0.57 x 0.50	E	Slight asymmetry in [N II]
SMP 46	5:19:29.72	-68:51:09.1	0.31	0.59 x 0.49	E(bc)	Ring?
SMP 53	5:21:32.93	-67:00:05.5	0.40	0.54 x 0.47	E(bc?)	Barrel shape, could be B
SMP 58	5:24:20.81	-70:05:01.9	0.13	0.23	R?	
SMP 59	5:24:27.43	-70:22:24.7	1.50	3.70 x 2.66	Q?	
SMP 65	5:27:43.92	-71:25:56.6	0.37	0.59	R	
SMP 71	5:30:33.22	-70:44:38.4	0.31	0.58 x 0.47	E	
SMP 78	5:34:21.31	-68:58:24.7	0.28	0.54 x 0.42	E(bc)	Barrel shape, could be B
SMP 79	5:34:08.76	-74:20:06.6	0.22	0.39 x 0.32	E(bc)	
SMP 80	5:34:38.87	-70:19:56.9	0.21	0.48	R	Ring in [N II]
SMP 81	5:35:20.92	-73:55:30.1	0.15	0.26	R?	
SMP 93	5:49:38.80	-69:10:00.1	1.43	3.6 x 3.0 6.4 x 3.0	B	Intersecting rings Faint extensions
SMP 94	5:54:10.77	-73:02:47.5	...	< 0.1	...	Unresolved; not a PN?
SMP 95	6:01:45.30	-67:56:08.0	0.46	1.15 x 0.95	E(bc)	With ansae
SMP 100	6:22:55.73	-72:07:41.4	0.71	1.36 x 1.18	E(bc) or Q?	
SMP 102	6:29:32.93	-68:03:32.9	0.71	1.06	R(bc?)	

^aSize excludes extended arms.

TABLE 3
 DIMENSIONS AND MORPHOLOGIES OF LMC PNE FROM WFPC2

Nebula	R_{Phot} (arcsec)	Dimensions (arcsec)	Morph. Class
SMP 1	0.18	0.33	R
SMP 15	0.41	0.75 x 0.61	E(bc)
SMP 33	0.31	0.67 x 0.57	E(bc)
SMP 38	0.25	0.57 x 0.40	E
SMP 41	1.47	3.56 x 1.86	B
SMP 42	0.46	0.83 x 0.67	Q(ES)
SMP 50	0.35	0.68 x 0.61	E(bc?)
SMP 52	0.41	0.75	R(bc?)
SMP 54	1.01	3.6 x 1.8	B
SMP 55	0.18	0.36	R
SMP 56	0.32	0.55	R
SMP 63	0.30	0.57 x 0.54	R
SMP 77	0.30	0.56 x 0.53	R
SMP 99	0.41	0.85 x 0.73	E(bc)

TABLE 4
 PN MORPHOLOGICAL TYPES: LMC VS. GALAXY

Morphological Class	LMC (Percent)	Galaxy ^a (Percent)
Elliptical (E)	17	49
Round (R)	29	23
Bi-Polar (B)	10	14
Bi-Polar Core (BC)	34	9
Quadrupolar (Q)	7	3
Point-Sym (P)	3	3
Total, Asymmetric ^b	51	26

^aDerived from the sample defined in Manchado, et al. (2000) and reclassified using the present scheme: see text.

^bIncludes types B, BC, and Q.

This figure "img1.gif" is available in "gif" format from:

<http://arxiv.org/ps/astro-ph/0010200v1>

This figure "img2.gif" is available in "gif" format from:

<http://arxiv.org/ps/astro-ph/0010200v1>

This figure "img3.gif" is available in "gif" format from:

<http://arxiv.org/ps/astro-ph/0010200v1>

This figure "img4.gif" is available in "gif" format from:

<http://arxiv.org/ps/astro-ph/0010200v1>

This figure "img5.gif" is available in "gif" format from:

<http://arxiv.org/ps/astro-ph/0010200v1>

This figure "img6.gif" is available in "gif" format from:

<http://arxiv.org/ps/astro-ph/0010200v1>

This figure "img7.gif" is available in "gif" format from:

<http://arxiv.org/ps/astro-ph/0010200v1>

This figure "img8.gif" is available in "gif" format from:

<http://arxiv.org/ps/astro-ph/0010200v1>

This figure "img9.gif" is available in "gif" format from:

<http://arxiv.org/ps/astro-ph/0010200v1>

This figure "img10.gif" is available in "gif" format from:

<http://arxiv.org/ps/astro-ph/0010200v1>

This figure "img11.gif" is available in "gif" format from:

<http://arxiv.org/ps/astro-ph/0010200v1>